ADVANCED MATERIALS
www.advmat.de

www.MaterialsViews.com

A New Class of Room-Temperature Multiferroic Thin Films with Bismuth-Based Supercell Structure

*Aiping Chen, Honghui Zhou, Zhenxing Bi, Yuanyuan Zhu, Zhiping Luo, Adrian Bayraktaroglu, Jamie Phillips, Eun-Mi Choi, Judith L. MacManus-Driscoll, Stephen J. Pennycook, Jagdish Narayan, Quanxi Jia, Xinghang Zhang, and Haiyan Wang**

Multiferroic materials, which exhibit the coexistence of ferromagnetism and ferroelectricity, have attracted extensive interest owing to their potential applications as multifunctional devices and fascinating physical phenomena.[1–3] Single-phase multiferroic materials are rare because of the distinct nature of magnetism, which is usually due to partially filled *d*-orbitals, while ferroelectricity commonly requires empty *d*-orbitals.[3] Interestingly, the multiferroics in the bismuth-based perovskites, such as $BiFeO_3$ (BFO) and $BiMnO_3$ (BMO), were achieved by separating magnetism and ferroelectricity in Fe^{3+}/Mn^{3+} and Bi^{3+} ions, respectively.[4] $BiFeO_3$ is one of the most well-studied room-temperature magnetic ferroelectrics with canted spin moments and large remanent polarization.[5,6] Its relatively low resistivity, caused by defects and non-stoichiometric compositions, gives rise to large leakage current in the devices.[7,8] Also, precise details of its magnetic properties are still under debate.[9–11] $BiMnO_3$ is one of the most promising multiferroics. However, it has a low magnetic Curie temperature (ca. 105 K), which in bulk form it requires high-pressure synthesis,[12,13] and in thin-film form it is hard to grow phase-pure.

Elemental doping by substitution has proven to be a successful approach to enhancing the physical properties of $BiFeO_3$. Various attempts by doping La^{3+} at Bi sites and Ni^{2+} and Mn^{3+} at Fe sites aim at reducing the leakage current and improving the ferroelectricity and piezoelectricity.[6–8,10,11] However, in addition to a weak magnetization at room temperature, it is quite difficult to optimize the growth conditions to enhance these parameters simultaneously.[6–8,10,11] Another approach to enhancing the multiferroicity is to integrate $BiFeO_3$ and a ferromagnetic material into a two-phase heteroepitaxial nanocomposite.[14] Nevertheless, only a few examples, with fine nano-checkerboard structure and large magnetoelectric coupling, have been reported.[15,16] Very recently, the combination of $BiFeO_3$ and $BiMnO_3$ has been investigated both experimentally and theoretically to achieve multifuntionality.[17–21] We have already demonstrated room-temperature magnetism in highly resistive, strained Bi_2FeMnO_6 thin films.[17,22] However, these films grow under a narrow set of growth conditions, and the functionalities exist within a limited thickness of less than ca. 40 nm. A robust single-phase multiferroic material with coexistent ferromagnetism and ferroelectricity at room temperature is highly desired.

Strain engineering provides an interesting and essential way to yield new materials with novel characteristics, such as the high pressure synthesis of cubic boron nitride,[23] and to tune the physical properties, such as improving the superconductivity and colossal magnetoresistance effect via the hydrostatic pressure and chemical pressure.[24,25] Compared with the strategies mentioned above, epitaxial strain arising from lattice mismatch could provide an easier and more flexible way to control the growth of strained films with enhanced physical properties.[26–30] In this study, we present a new class of room-temperature multiferroics based on two partially miscible phases of $BiFeO_3$ and $BiMnO_3$, with a new structure enabled by epitaxial strain. The new BFMO single phase shows a bismuth supercell (SC) structure on $LaAlO_3$ (LAO) substrates and exhibits both ferrimagnetic and ferroelectric responses at room temperature. More interestingly, this new phase can be formed on other substrates with a properly selected buffer layer.

A. P. Chen, Dr. Z. X. Bi, Y. Y. Zhu, Prof. H. Y. Wang
Department of Electrical and Computer Engineering
Texas A&M University
College Station, TX 77843-3128, USA
E-mail: wangh@ece.tamu.edu
Dr. H. H. Zhou, Dr. S. J. Pennycook
Materials Science & Technology Division
Oak Ridge National Laboratory, Oak Ridge, TN 37831, USA
Dr. H. H. Zhou, Prof. J. Narayan
Department of Materials Science and Engineering
NSF Center for Advanced Materials and Smart Structures
North Carolina State University
Raleigh, NC 27695, USA
Dr. Z. P. Luo
Department of Chemistry and Physics
Fayetteville State University
Fayetteville, NC 28301, USA and Microscopy and Imaging Center
Texas A&M University
College Station, TX 77843, USA
A. Bayraktaroglu, Prof. J. Phillips
Department of Electrical Engineering and Computer Science
The University of Michigan
Ann Arbor, MI 48109, USA
Dr. E.-M. Choi, Dr. J. L. MacManus-Driscoll
Department of Materials Science and Metallurgy
University of Cambridge
Pembroke Street, Cambridge, CB2 3QZ, UK
Dr. Q. X. Jia
Center for Integrated Nanotechnologies (CINT)
Los Alamos National Laboratory
Los Alamos, NM 87545, USA
Prof. X. H. Zhang
Department of Mechanical Engineering
Texas A&M University
College Station, TX 77843, USA

DOI: 10.1002/adma.201203051

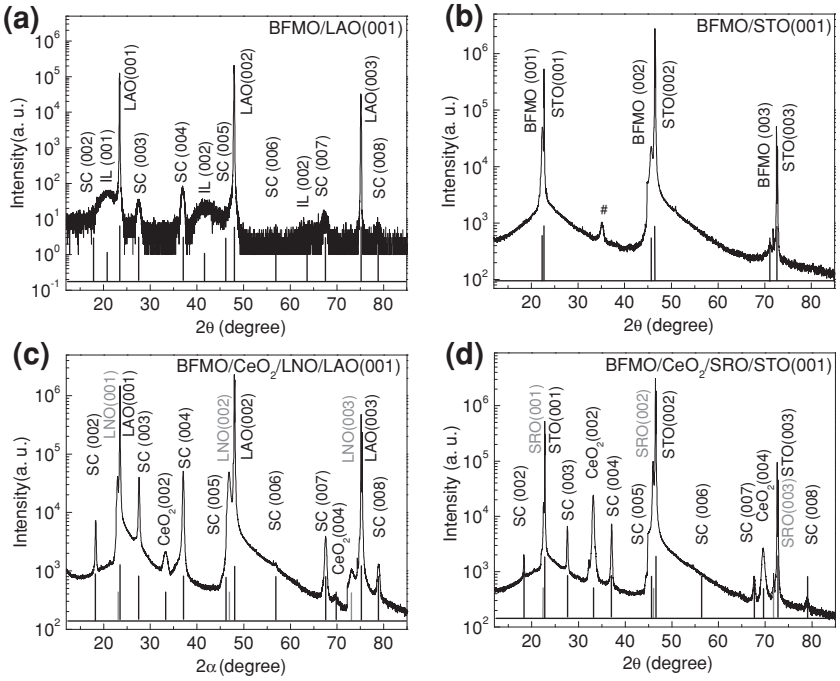

Figure 1. XRD patterns of the new BFMO SC structure. a) XRD (θ–2θ) scan shows three sets of (00l)-type peaks, corresponding to the self-assembled BFMO bilayer film and the LAO substrate. SC and IL indicate the film with the bismuth SC structure and the thin interlayer with pseudo-perovskite structure, respectively. b) XRD scan of BFMO films directly grown on STO substrate with pseudo-perovskite structure. The "#" is an impurity phase. c) BFMO SC films grown on CeO_2-buffered $LaNiO_3$/LAO substrates. d) BFMO SC films grown on CeO_2-buffered $SrRuO_3$/STO substrates. The vertical lines at the bottom of the XRD graphs indicate the peak locations.

The new BFMO SC structure was first observed in the X-ray diffraction (XRD) pattern of the as-deposited thin films on LAO substrates. As shown in **Figure 1**a, other than the diffractions from the substrate, two sets of film (00l) peaks were observed in the typical θ–2θ scans, indicating that this BFMO thin film has grown in a highly textured manner. The out-of-plane d-spacings of the BFMO film were determined to be 4.39 Å and 4.85 Å, for the diffraction set with broadened peaks (at 2θ = 20.21°, 41.61°, and 62.88°) and for the diffraction set with sharp peaks (at 2θ = 18.28°, 27.57°, 36.96°,…), respectively. The d-spacing of the first set of diffraction peaks roughly matched (but highly strained and later identified as originating from an interlayer, IL) the lattice parameters reported in previous BFMO epitaxial films;[17,31] however, the out-of-plane d-spacing of the second set of the diffraction peaks does not fit any of the well-known BFMO phases. Therefore, a new phase exists in the sample, which we call the supercell (SC) hereafter (Figure 1a). In addition, the sharp peaks exhibit stronger diffraction intensity, suggesting the new phase (SC) represents the majority portion of the epitaxial film. It is also noted that this set of unknown diffractions was found in the BFMO films directly grown on LAO substrates, but not those directly grown on $SrTiO_3$ (STO) substrates (Figure 1b). More interestingly, this new structure can also be grown nicely on CeO_2-buffered LAO or STO substrates, as shown in Figures 1c,d (also see Supporting information).

Aberration-corrected scanning transmission electron microscopy (STEM) in high-angle annular dark-field (HAADF) mode was conducted on the BFMO films directly grown on STO and LAO substrates along the substrate [100] zone axis, and the representative images are shown in **Figure 2**. Although the films were grown under identical deposition conditions, they present distinctly different structures. The HAADF-STEM images provide atomic arrangements of the cation sublattice at the heterogeneous interfaces (note that the O columns are not resolvable in these STEM images). Since the recorded intensity is proportional to Z^n ($1.5 \le n \le 2$), the STO substrate along the [100] axis presents a typical perovskite lattice, consisting of Sr columns (bright), and the less bright Ti–O columns located in the centers of the Sr square lattice (the left-hand inset of Figure 2a). The BFMO on STO exhibits a biaxial strained pseudo-perovskite structure with lattice parameters a = 3.93 Å and c = 3.99 Å, in agreement with the previously reported tetragonal structure.[17] The BFMO on the LAO substrate, however, shows an interesting SC structure along the c-axis with a thin self-assembled IL between the BFMO SC layer and the substrate (Figure 2b). This SC structure is completely different from any previously reported vertically aligned nanocomposite, even though similar deposition methods and conditions were used.[28–30,32,33] Figure 2c shows the IL structure between the

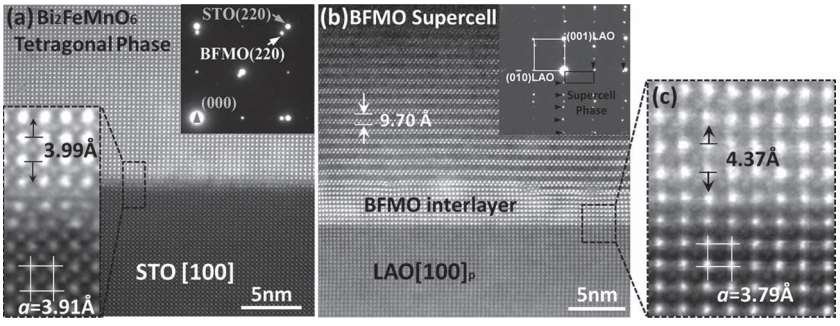

Figure 2. STEM images of BFMO films on STO and LAO substrates under the same deposition conditions. a) Cross-sectional STEM image at the substrate and film interface for a typical BFMO film grown on STO substrate. b) Cross-sectional STEM image of a typical BFMO film grown on the LAO substrate showing two layers, i.e., a coherent highly strained interface layer (this IL resembles the pseudo-perovskite BFMO on STO with a = 3.80 Å and c = 4.37 Å) and a bismuth SC layer. Bottom left corner inset in (a): A higher magnification image of the outlined region in (a). Top right corner insets in (a,b): Selected area electron diffraction (SAED) patterns of BFMO films taken by TEM for the samples on STO (a) and LAO (b). c) Higher magnification image of the outlined region in (b) showing the coherent interface between the LAO substrate and the BFMO strained interlayer.

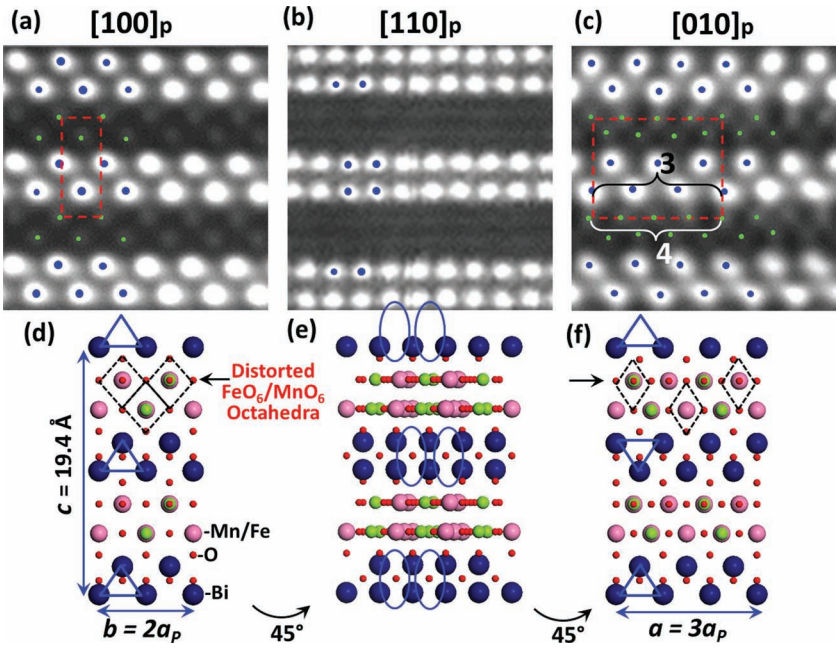

Figure 3. STEM images and the corresponding atomic model of the BFMO322 SC films. a–c) Cross-sectional high-resolution STEM images of BFMO322 SC films along the $[100]_P$ (a), $[110]_P$ (b), and $[010]_P$ (c) zone axes. d–f) The atomic modeling of the new BMFO phase along the $[100]_P$ (d), $[110]_P$ (e), and $[010]_P$ (f) zone axes.

SC and the substrate. Although the IL resembles the pseudo-perovskite BFMO on STO, a careful lattice measurement results in a = 3.80 Å and c = 4.37 Å (the c lattice parameter agrees well with that of the minor diffraction set in XRD, Figure 1a) which suggests an even larger in-plane compression and out-of-plane tension with c/a = 1.15 Å. This highly strained BFMO IL is very thin, in the range of 3–5 nm, measured from different regions along the film/substrate interface. The novel SC layer forms on top of the thin IL.

Along the pseudo-perovskite [100] zone axis ($[100]_P$, the axis is used here for the purpose of easy illustration and not the actual axis of SC structure) in the SC film (Figure 2b and enlarged view in **Figure 3**a), the HAADF-STEM image presents stripes consisting of triangles of obviously bright dots, which are identified as Bi_2O_2 sheets, which commonly exist in other bismuth oxy-compounds.[34] The spacing between the neighboring Bi_2O_2 sheets is about 9.70 Å (about twice the d-spacing of the SC (002) peak observed in Figure 1a). This confirms that the dominant diffraction peaks (SC peaks) detected by XRD correspond to the SC structure. The electron diffraction pattern of the SC along the $[100]_P$ zone (inset in Figure 2b), showing periodic out-of-plane diffractions with large lattice spacing, also confirms such a SC structure besides the diffraction dots from LAO. Energy dispersive X-ray analysis (EDX) further revealed that the cation ratio of this BFMO SC layer is Bi:Fe:Mn = 3:2:2 (called BFMO322 SC) (see Supporting Information). Figure 3 shows the HAADF STEM images of the BFMO322 SC along all three major zone axes, among them both $[100]_P$ and $[010]_P$ were acquired along the LAO [100] zone axis. In the $[100]_P$ zone (Figure 3a), the neighboring Bi_2O_2 sheets are at the same location along the horizontal direction *b*. However in $[110]_P$ and $[010]_P$ zones, as shown in Figures 3b and c, respectively, the Bi_2O_2 sheets are offset by half a period along the horizontal direction. Between the neighboring Bi_2O_2 sheets are two layers of Fe-O/Mn-O, which have a similar triangle-stripe feature (consisting of weak dots) matching the Bi_2O_2 lattice 1:1 along the $[100]_P$ zone axis but 4:3 under the $[010]_P$ zone axis. Thus, the BFMO322 SC structure with $a = 2a_P$ (a_P stands for the lattice parameter of the pseudo-perovskite BFMO phase), $b = 3a_P$ (a_P ~ 3.99 Å) and c ~ 19.40 Å, as illustrated in Figures 3d–f, is proposed for the observed BFMO322 SC structure. Starting with a tetragonal structure (an Aurivillius phase Bi_2WO_6,[35] see Supporting Information), the neighboring Bi_2O_2 sheets were shifted along the a direction by half a period (a/2), resulting in the offset of bismuth layer configurations along $[110]_P$ and $[010]_P$. A commensurate modulation in the Fe-O/Mn-O double layers leads to an overlapped layer between the Bi_2O_2 sheets along the projection view along $[110]_P$, which is consistent with the experimental result (Figure 3b). It should be noted that this SC structure gives the consistent composition of Bi:Fe:Mn = 3:2:2 as observed by the EDX study, and the simulated diffraction patterns from different zones match the experimental diffraction patterns well.

The growth mechanism of this novel BFMO322 SC structure, though still under further investigation, is likely to be attributed to two aspects. On the one hand, Aurivillius phase (Bi_2O_2)($A_{m-1}B_mO_{3m+1}$), possessing a large family of intergrowth structures (m = 1 to 8), could be the structural origin of the SC. Interestingly, the stacking modulation observed in the SC structure occurs in the $[A_{m-1}B_mO_{3m+1}]^{2-}$ perovskite-like blocks, where the two intergrowth structures become distinct from each other. On the other hand, the comparative study by growing the films on the STO substrates under the same conditions suggests a strong substrate dependence for the formation of the SC structure. The LAO substrate presents a much larger lattice misfit (ca. –2.0%) with the expected $BiFe_{0.5}Mn_{0.5}O_3$ orthorhombic phase[21] than that of the STO case (ca. –0.6%). The lattice strain effects on the pseudo-perovskite BFMO interlayer on LAO are quite obvious in terms of the degree of unit cell anisotropy, c/a = 1.15; whereas, the ratio c/a is close to 1 (ca. 1.02) in the BFMO on STO. Thus, it is quite likely that the relaxation of larger biaxial strain, induced by the LAO substrate, in the BFMO IL triggers the layered bismuth compound stacking disordering, thus forming the new SC structure. It should be pointed out that strain-induced coexistence of T and R phases in BFO films has been reported with a reversible temperature-induced phase transition close to room temperature when they were compressively grown on LAO substrates.[36,37] Our results as well as previous reports all suggest that the substrate-induced epitaxial strain is an important approach to yield new structures with new functionality.

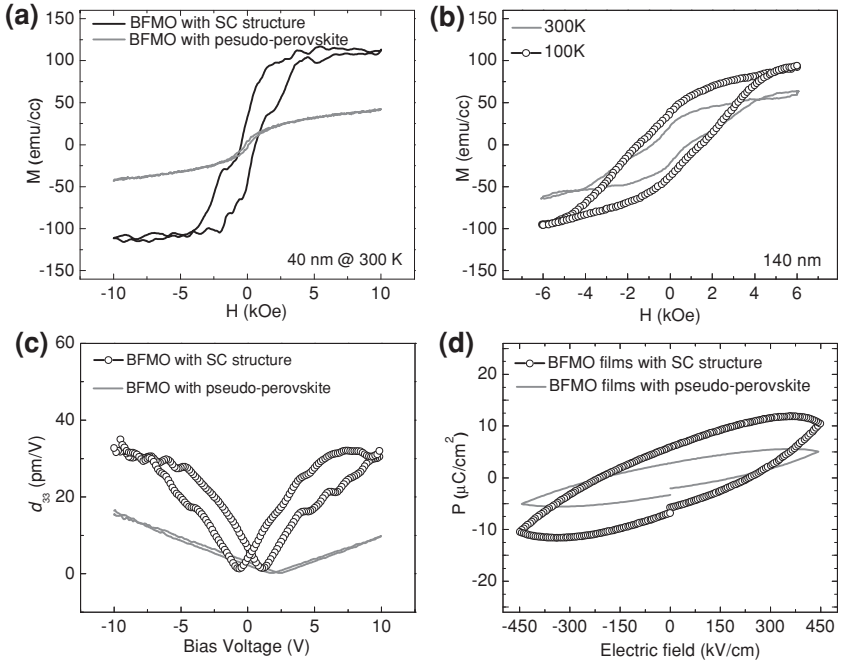

Figure 4. Room temperature multiferroic properties in BFMO322 SC films. a) Room-temperature in-plane magnetic hysteresis loop (*M–H*) of 40 nm BFMO films deposited on LAO (black curve) and STO (gray curve) substrates. b) *M–H* (out-of-plane) of 140 nm BFMO332 SC films on CeO_2/STO at 100 K (circles) and 300 K (line). c) Piezoelectric coefficient d_{33} versus bias voltage hysteresis loops with bismuth SC structure and the BFMO with regular pseudo-perovskite structure. d) The polarization–electric field (*P–E*) hysteresis loops of BFMO films on bismuth with (circles) and without (line) SC structure.

Based upon our experimental observations, it is clear that BFMO on LAO grows first pseudomorphically as the BFMO IL with $a = b = 3.80$ Å, matching the interfacial substrate lattice constants. Above the critical thickness of 3–5 nm, the strain energy builds up and a new equilibrium structure, that is, the BFMO322 SC structure, is formed. This new phase is a relaxed structure with misfit dislocations accommodating the strain between the new phase and the pseudomorphic transition layer (IL). The misfit between the new phase and the pseudomorphic transition layer is large enough that critical thickness is within the *c*-unit cell dimension normal to the interface. Similar intermediate pseudomorphic structures have been observed previously in $TiO_2/Ti_2O_3/Al_2O_3$ and $VO_2/V_2O_3/Al_2O_3$ heterostructures, which follow the domain-matching-epitaxy paradigm for epitaxy between the pseudomorphic transition layer and the equilibrium phase under large misfit conditions.[38–40]

The realization of the BFMO322 SC structure provides a new clue as to how to grow fascinating new phases with high substrate/film misfit, including new single-phase multiferroic materials. **Figure 4**a shows the room temperature magnetic hysteresis loops of BFMO films deposited on either a LAO or a STO substrate. It clearly shows the room temperature saturated magnetization is ca. 110 emu/cc (ca. 1.1×10^5 A m^{-1} as 1 emu/cc = 10^3 A m^{-1}) for the 40 nm BFMO322 SC on LAO, which is larger than the BFMO films directly deposited on STO in this work (34 emu/cc) and many other reports of BFO films (3–40 emu/cc).[6–8,10,11] Figure 4b shows the well-defined out-of-plane magnetic hysteresis loops of a 140 nm BFMO322 SC structure film on CeO_2-buffered STO at 100 K and 300 K. The larger coercivity and remanent magnetization at lower temperatures in BFMO322 SC structure films are typical characteristics of ferrimagnetic materials. Similar to the weak ferromagnetism in BFO, the small magnetic response in BFMO regular perovskite phase is likely due to the spin canting effect.[41] The stronger ferrimagnetism in BFMO322 SC structure films possibly arises from the modulated novel structure. The atomic models suggest that the Mn and Fe cations form zigzag-shaped rows (Figures 3d–f), which may favor the spin canting effect. The commensurate modulation in the Fe-O/Mn-O double layers and stacking modulation would lower the crystal symmetry to monoclinic. This may result in a net magnetic moment in this new structure. To confirm the ferroelectric properties of the SC-structured BFMO322 thin films, piezoelectric properties and polarization–electric field (*P–E*) hysteresis loops have been measured at room temperature (Figures 4c,d). The effective piezoelectric coefficient d_{33} was calculated to be ca. 30 pm V^{-1} for the BFMO322 thin films with the SC structure, which is much larger than that of BFMO thin films with pseudo-perovskite structure. The remanent polarizations P_r, as shown in Figure 4d, are 6 μC cm^{-2} and 2.7 μC cm^{-2} for the BFMO thin films with the bismuth SC and pseudo-perovskite structure, respectively. Even though the P_r of BFMO322 SC thin films is still much lower than that of some of the reported BFO films (60–80 μC cm^{-2}),[7,8,10,11] the BFMO322 SC thin films exhibit greatly enhanced room temperature magnetization (ca. 110 emu/cc) compared to BFO films (<40 emu/cc).[7–10] Our results indicate that the integration — through the epitaxial strain — of the two partially miscible phases of BFO and BMO into a new phase with double rows of Fe/Mn in zigzag arrangement could be a very useful and unique way to develop new multiferroic materials. The strongly distorted (FeO_6/MnO_6) octahedra in the Fe-O/Mn-O slabs (Figures 3d,f), may result from the commensurate and stacking modulations between Fe/Mn double rows (Fe-O/Mn-O) and the double bismuth layers (Bi_2O_2 sheets). The ferrimagnetic response may come from the spin canting effect in the modulated structure. The non-centrosymmetric nature resulting from the stacking and commensurate modulations may contribute to the ferroelectric behavior in this BFMO322 SC-structured multiferroic. These findings should encourage further efforts to deepen understanding of and to improve multiferroics with this new SC structure.

In summary, epitaxial BFMO322 thin films with SC structure have been grown on LAO substrates with a thin pseudo-perovskite BFMO interlayer. The new structure demonstrates both room-temperature ferrimagnetic and ferroelectric responses. The STEM results show the unique bismuth SC structures interlayered with double-row Fe-O-Mn layers with a zigzag arrangement. The new structure possibly favors the

spin canting effect, which could be responsible for the observed magnetism, while the non-centrosymmetric nature of the new structure permits the ferroelectric behavior. More interestingly, the integration of two partially miscible multiferroic materials by means of strain confinement opens a new route to developing single-phase thin films with room temperature multiferroic properties. This demonstration will stimulate further work exploring new single-phase multiferroic thin films by proper intermixing of two perovskite $BiRO_3$ (R = Cr, Mn, Fe, Co, Ni) materials.

Supporting Information

Supporting Information is available from the Wiley Online Library or from the author.

Acknowledgements

A.P.C., H.H.Z., and Z.X.B. contributed equally to this work. This work was supported by the U.S. National Science Foundation (NSF-1007969 and NSF-0846504). Q.X.J. acknowledges the support of the U.S. Department of Energy through the LANL/LDRD program and the Center for Integrated Nanotechnologies (CINT) for this work. J.N. thanks the U.S. National Science Foundation (NSF-080366) and Army Research Office for support. S.J.P. was supported by the U.S. Department of Energy, Basic Energy Sciences, Materials Sciences and Engineering Division. J.L.M.-D thanks the ERC for an Advanced Investigator Grant, Novox, ERC-2009-adG 247276 and the EPSRC (UK) for grant EP/H047867/1. A.P.C. thanks the Office of Graduate Studies of Texas A&M University for support through a Dissertation Fellowship.

Received: July 26, 2012
Revised: October 12, 2012
Published online: November 26, 2012

[1] N. A. Hill, *J. Phys. Chem. B* **2000**, *104*, 6694.
[2] R. Ramesh, N. A. Spaldin, *Nat. Mater.* **2007**, *6*, 21.
[3] S. W. Cheong, M. Mostovoy, *Nat. Mater.* **2007**, *6*, 13.
[4] D. I. Khomskii, *J. Magn. Magn. Mater.* **2006**, *306*, 1.
[5] J. Wang, J. B. Neaton, H. Zheng, V. Nagarajan, S. B. Ogale, B. Liu, D. Viehland, V. Vaithyanathan, D. G. Schlom, U. V. Waghmare, N. A. Spaldin, K. M. Rabe, M. Wuttig, R. Ramesh, *Science* **2003**, *299*, 1719.
[6] X. D. Qi, J. Dho, R. Tomov, M. G. Blamire, J. L. MacManus-Driscoll, *Appl. Phys. Lett.* **2005**, *86*, 062903.
[7] Y. H. Lee, J. M. Wu, C. H. Lai, *Appl. Phys. Lett.* **2006**, *88*, 042903.
[8] S. K. Singh, K. Maruyama, H. Ishiwara, *Appl. Phys. Lett.* **2007**, *91*, 112913.
[9] W. Eerenstein, F. D. Morrison, J. Dho, M. G. Blamire, J. F. Scott, N. D. Mathur, *Science* **2005**, *307*, 1203.
[10] J. Z. Huang, Y. Wang, Y. Lin, M. Li, C. W. Nan, *J. Appl. Phys.* **2009**, *106*, 063911.
[11] F. Yan, T. J. Zhu, M. O. Lai, L. Lu, *Scr. Mater.* **2010**, *63*, 780.
[12] W. Eerenstein, F. D. Morrison, F. Sher, J. L. Prieto, J. P. Attfield, J. F. Scott, N. D. Mathur, *Philos. Mag. Lett.* **2007**, *87*, 249.
[13] R. Seshadri, N. A. Hill, *Chem. Mater.* **2001**, *13*, 2892.
[14] H. Zheng, J. Wang, S. E. Lofland, Z. Ma, L. Mohaddes-Ardabili, T. Zhao, L. Salamanca-Riba, S. R. Shinde, S. B. Ogale, F. Bai, D. Viehland, Y. Jia, D. G. Schlom, M. Wuttig, A. Roytburd, R. Ramesh, *Science* **2004**, *303*, 661.
[15] Z. P. Tan, J. Slutsker, A. L. Roytburd, *J. Appl. Phys.* **2009**, *105*, 061615.
[16] L. Yan, Z. G. Wang, Z. P. Xing, J. F. Li, D. Viehland, *J. Appl. Phys.* **2010**, *107*, 064106.
[17] E. M. Choi, S. Patnaik, E. Weal, S. L. Sahonta, H. Wang, Z. Bi, J. Xiong, M. G. Blamire, Q. X. Jia, J. L. MacManus-Driscoll, *Appl. Phys. Lett.* **2011**, *98*, 012509.
[18] L. Bi, A. R. Taussig, H. S. Kim, L. Wang, G. F. Dionne, D. Bono, K. Persson, G. Ceder, C. A. Ross, *Phys. Rev. B* **2008**, *78*, 104106.
[19] P. Mandal, A. Sundaresan, C. N. R. Rao, A. Iyo, P. M. Shirage, Y. Tanaka, C. Simon, V. Pralong, O. I. Lebedev, V. Caignaert, B. Raveau, *Phys. Rev. B* **2010**, *82*, 100416.
[20] L. Palova, P. Chandra, K. M. Rabe, *Phys. Rev. B* **2010**, *82*, 075432.
[21] M. Azuma, H. Kanda, A. A. Belik, Y. Shimakawa, M. Takano, *J. Magn. Magn. Mater.* **2007**, *310*, 1177.
[22] E.-M. Choi, T. Fix, A. Kursumovic, C. Kinane, D. Arena, S.-L. Sahonta, Z. Bi, J.-S. Lee, H. Wang, S. Langridge, M. G. Blamire, Q. Jia, J. L. MacManus-Driscoll, unpublished.
[23] P. F. McMillan, *Nat. Mater.* **2002**, *1*, 19.
[24] M. Mito, M. J. Pitcher, W. Crichton, G. Garbarino, P. J. Baker, S. J. Blundell, P. Adamson, D. R. Parker, S. J. Clarke, *J. Am. Chem. Soc.* **2009**, *131*, 2986.
[25] M. Uehara, S. Mori, C. H. Chen, S. W. Cheong, *Nature* **1999**, *399*, 560.
[26] D. G. Schlom, L.-Q. Chen, C.-B. Eom, K. M. Rabe, S. K. Streiffer, J.-M. Triscone, *Annu. Rev. Mater. Res.* **2007**, *37*, 589.
[27] R. J. Zeches, M. D. Rossell, J. X. Zhang, A. J. Hatt, Q. He, C. H. Yang, A. Kumar, C. H. Wang, A. Melville, C. Adamo, G. Sheng, Y. H. Chu, J. F. Ihlefeld, R. Erni, C. Ederer, V. Gopalan, L. Q. Chen, D. G. Schlom, N. A. Spaldin, L. W. Martin, R. Ramesh, *Science* **2009**, *326*, 977.
[28] J. L. MaCmanus-Driscoll, P. Zerrer, H. Y. Wang, H. Yang, J. Yoon, A. Fouchet, R. Yu, M. G. Blamire, Q. X. Jia, *Nat. Mater.* **2008**, *7*, 314.
[29] S. A. Harrington, J. Y. Zhai, S. Denev, V. Gopalan, H. Y. Wang, Z. X. Bi, S. A. T. Redfern, S. H. Baek, C. W. Bark, C. B. Eom, Q. X. Jia, M. E. Vickers, J. L. MacManus-Driscoll, *Nat. Nanotechnol.* **2011**, *6*, 491.
[30] Z. X. Bi, J. H. Lee, H. Yang, Q. X. Jia, J. L. MacManus-Driscoll, H. Y. Wang, *J. Appl. Phys.* **2009**, *106*, 094309.
[31] J. Miao, X. Zhang, Q. Zhan, Y. Jiang, K. H. Chew, *Appl. Phys. Lett.* **2011**, *99*, 062905.
[32] A. P. Chen, Z. X. Bi, C. F. Tsai, J. Lee, Q. Su, X. H. Zhang, Q. X. Jia, J. L. MacManus-Driscoll, H. Y. Wang, *Adv. Funct. Mater.* **2011**, *21*, 2423.
[33] A. P. Chen, Z. X. Bi, H. Hazariwala, X. H. Zhang, Q. Su, L. Chen, Q. X. Jia, J. L. MacManus-Driscoll, H. Y. Wang, *Nanotechnology* **2011**, *22*, 315712.
[34] B. Frit, J. P. Mercurio, *J. Alloys Compd.* **1992**, *188*, 27.
[35] R. W. Wolfe, R. E. Newnahm, M. I. Kay, *Solid State Commun.* **1969**, *7*, 1797.
[36] I. C. Infante, J. Juraszek, S. Fusil, B. Dupe, P. Gemeiner, O. Dieguez, F. Pailloux, S. Jouen, E. Jacquet, G. Geneste, J. Pacaud, J. Iniguez, L. Bellaiche, A. Barthelemy, B. Dkhil, M. Bibes, *Phys. Rev. Lett.* **2011**, *107*, 237601.
[37] J. Kreisel, P. Jadhav, O. Chaix-Pluchery, M. Varela, N. Dix, F. Sanchez, J. Fontcuberta, *J. Phys. Condens. Matter* **2011**, *23*, 342202.
[38] S. H. Baek, J. Park, D. M. Kim, V. A. Aksyuk, R. R. Das, S. D. Bu, D. A. Felker, J. Lettieri, V. Vaithyanathan, S. S. N. Bharadwaja, N. Bassiri-Gharb, Y. B. Chen, H. P. Sun, C. M. Folkman, H. W. Jang, D. J. Kreft, S. K. Streiffer, R. Ramesh, X. Q. Pan, S. Trolier-McKinstry, D. G. Schlom, M. S. Rzchowski, R. H. Blick, C. B. Eom, *Science* **2011**, *334*, 958.
[39] J. Narayan, B. C. Larson, *J. Appl. Phys.* **2003**, *93*, 278.
[40] M. R. Bayati, R. Molaei, R. J. Narayan, J. Narayan, H. Zhou, S. J. Pennycook, *Appl. Phys. Lett.* **2012**, *100*, 251606.
[41] G. Catalan, J. F. Scott, *Adv. Mater.* **2009**, *21*, 2463.